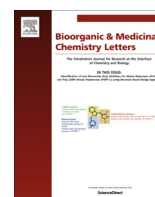




Contents lists available at ScienceDirect

Bioorganic & Medicinal Chemistry Letters

journal homepage: www.elsevier.com/locate/bmcl

Virtual screen to NMR (VS2NMR): Discovery of fragment hits for the CBP bromodomain



Dimitrios Spiliotopoulos^{a,*}, Jian Zhu^a, Eike-Christian Wamhoff^{b,c}, Nicholas Deerain^a, Jean-Rémy Marchand^a, Jonas Aretz^{b,c}, Christoph Rademacher^{b,c}, Amedeo Caffisch^{a,*}

^a Department of Biochemistry, University of Zürich, Winterthurerstrasse 190, CH-8057 Zürich, Switzerland

^b Department of Biomolecular Systems, Max Planck Institute of Colloids and Interfaces, Am Mühlenberg 1, 14424 Potsdam, Germany

^c Institute of Chemistry and Biochemistry, Department of Biology, Chemistry, and Pharmacy, Freie Universität Berlin, Takustraße 3, 14195 Berlin, Germany

ARTICLE INFO

Article history:

Received 7 February 2017

Revised 31 March 2017

Accepted 1 April 2017

Available online 4 April 2017

Keywords:

Docking
Virtual screening
NMR spectroscopy
Epigenetics
X-ray crystallography
Bromodomain inhibitors

ABSTRACT

Overexpression of the CREB-binding protein (CBP), a bromodomain-containing transcription coactivator involved in a variety of cellular processes, has been observed in several types of cancer with a correlation to aggressiveness. We have screened a library of nearly 1500 fragments by high-throughput docking into the CBP bromodomain followed by binding energy evaluation using a force field with electrostatic solvation. Twenty of the 39 fragments selected by virtual screening are positive in one or more ligand-observed nuclear magnetic resonance (NMR) experiments. Four crystal structures of the CBP bromodomain in complex with *in silico* screening hits validate the pose predicted by docking. Thus, the success ratio of the high-throughput docking procedure is 50% or 10% if one considers the validation by ligand-observed NMR spectroscopy or X-ray crystallography, respectively. Compounds **1** and **3** show favorable ligand efficiency in two different *in vitro* binding assays. The structure of the CBP bromodomain in the complex with the brominated pyrrole **1** suggests fragment growing by Suzuki coupling.

© 2017 Elsevier Ltd. All rights reserved.

Bromodomains are protein-protein interaction modules that bind acetylated lysine (Kac)¹ or other acyl modifications of the lysine side chain.² The bromodomain fold consists of a left-handed four-helix bundle (helices Z, A, B, and C) with the interhelical loops ZA and BC flanking the rim of the acetyllysine-binding pocket.^{3,4} The potential involvement of bromodomains in several types of cancer and inflammatory diseases⁵ sparked interest in developing small molecules inhibiting their Kac-binding activity.⁶

The bromodomain of the lysine acetyltransferase CBP (the binding protein of the cyclic-AMP response element binding protein)

Abbreviations: Alpha, amplified luminescent proximity homogeneous assay; ATAD2, ATAD2 ATPase family, AAA domain containing 2; BAZ2A, bromodomain adjacent to zinc finger domain protein 2A; BAZ2B, bromodomain adjacent to zinc finger domain protein 2B; BRPF1, bromodomain and PHD finger (BRPF) containing protein 1; CBP, CREB-binding protein; CREB, cyclic-AMP response element binding protein; CSPs, chemical shift perturbations; DMSO, dimethyl sulfoxide; DSF, differential scanning fluorimetry; EP300, adenoviral E1A binding protein; HAC, heavy atom count; Kac, N-ε-acetyllysine; LE, ligand efficiency; NMR, nuclear magnetic resonance; qPCR, quantitative PCR polymerase chain reaction; STD, saturation transfer difference; VS2NMR, Virtual Screen to NMR.

* Corresponding authors.

E-mail addresses: d.spiliotopoulos@bioc.uzh.ch (D. Spiliotopoulos), caffisch@bioc.uzh.ch (A. Caffisch).

<http://dx.doi.org/10.1016/j.bmcl.2017.04.001>

0960-894X/© 2017 Elsevier Ltd. All rights reserved.

has been the object of intense investigations due to the role of CBP in several cellular processes and implication in cancer.⁷ Small-molecule ligands of the CBP bromodomain have been discovered by others using *in vitro* screening techniques^{8–12} and in our research group by *in silico* screening (high-throughput docking).¹³ The latter have been optimized by medicinal chemistry into potent and selective CBP bromodomain inhibitors.¹⁴

Here we report on the identification of ligand-efficient CBP bromodomain inhibitors via the computational screening of nearly 1500 small molecules. As a point of departure with respect to our previous virtual screening campaigns on CBP, here we take advantage of ligand-based NMR spectroscopy to validate the docking results. We call the sequential *in silico* to *in vitro* strategy Virtual Screen to NMR (VS2NMR).

In an effort to identify ligand-efficient small molecule inhibitors of the CBP bromodomain, we performed a rigid-ligand docking screen taking advantage of the software SEED.^{16,17} A library of 1413 small molecules was docked into the acetyllysine binding site of the CBP bromodomain (Figs. 1 and S1) and the binding energy of the resulting poses was calculated using a force field-based energy function with approximation of desolvation effects in the continuum-dielectric representation.^{16,17} The docked poses of the frag-

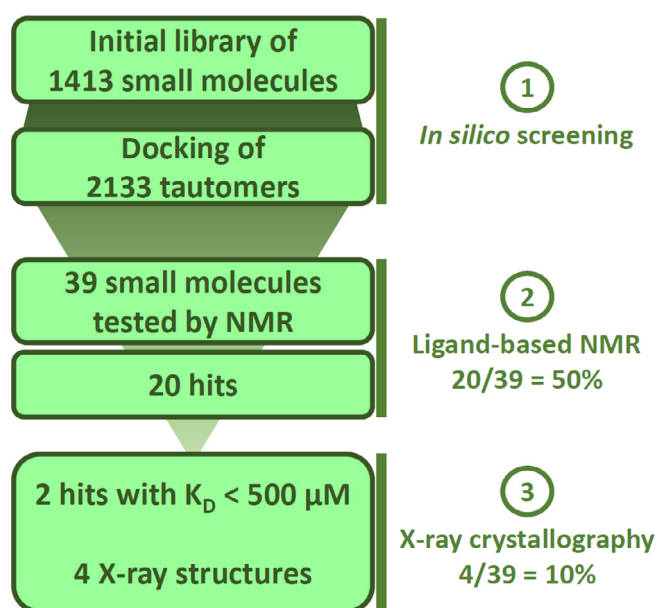


Fig. 1. Flowchart of the VS2NMR workflow and subsequent experimental validation by means of competition binding assays and X-ray crystallography. VS2NMR consisted of (1) virtual screening by high-throughput fragment docking using the program SEED^{16,17} and (2) ligand-based NMR spectroscopy. This efficient screening strategy was finally validated by (3) two different *in vitro* binding assays^{15,22} and X-ray crystallography. The success ratio of the *in silico* screening is 50% according to ligand-observed NMR spectroscopy and 10% according to X-ray crystallography.

ments were filtered to enforce a hydrogen bond with the conserved water molecule w_1 (Fig. S1) that bridges to the side chain hydroxyl of the conserved Tyr1125 (see Supplementary information). The remaining poses were ranked according to the median rank of a consensus scoring aimed to prioritize molecules with favorable electrostatic contribution to the binding energy (including desolvation penalties) and van der Waals interactions. Of the 60 selected fragments, 39 were ultimately chosen to be validated via NMR techniques (Table S1) based on results from experimental quality control.¹⁸

To experimentally validate these fragments as ligands of the CBP bromodomain, we took advantage of ligand-based NMR spectroscopy. The *in silico* hits were divided into four mixtures of 9–10 molecules each with minimal ¹H NMR spectral overlap. Fragments which displayed a clear evidence for binding in at least one of three ligand-observed NMR spectroscopy experiments, *viz.*, ¹H, STD, and R_2 -filtered,^{19,20} were selected for further validation. To ensure specificity for the primary binding site we included competition experiments with SGC-CBP30, a nanomolar ligand of the CBP bromodomain⁸ (Fig. S2). Overall, specific interactions with the CBP bromodomain were observed for 20 of the 39 small molecules, which corresponds to a success ratio (defined as the quotient of true positives divided by the number of compounds tested by NMR) of 50% for the *in silico* screening (Fig. 1). The most pronounced effects were observed for compounds **1–4** (Table 1), showing STD effects as well as chemical shift perturbation (CSPs) and enhanced R_2 relaxation in presence of CBP (Table 2).

To further validate the 20 compounds that showed binding in the ligand-observed NMR experiments, competition binding assays were performed first with the AlphaScreen technology using a tetra-acetylated peptide segment from the histone H4. At 0.5 mM compound concentration, 50% or higher inhibition of the CBP bromodomain was observed for five of the 20 actives in the NMR experiments (Table 2). Two of these compounds were not investigated further because of lack of novelty of their head group. These are the 3-acetylindole **2**, which is similar to a fragment recently

disclosed as a 29- μM inhibitor of the BRPF1 bromodomain,²¹ and the acetylbenzene derivative **4**, which shares the same head group as our previously disclosed CBP inhibitors.^{13,14} Furthermore, the pyrazole derivative **5** was discarded because of its poor affinity, also confirmed by the lack of shift in the DSF assay (Table 1). The remaining two compounds (**1** and **3**) displayed micromolar affinity in dose-response measurements using two different biochemical assays (Table 1 and Fig. S3). The IC_{50} values measured by the AlphaScreen approach²² are about one order of magnitude less favorable than the K_D values obtained by a competition binding assay based on DNA-tagged CBP bromodomain and PCR quantification.¹⁵ Such discrepancies have already been reported in previous studies of bromodomain ligands.^{23–25} They are likely to originate from different experimental conditions, protocols, and/or the use of different competitor molecules (the AlphaScreen assay was performed using a tetra-acetylated 21-mer H4 peptide whereas a proprietary undisclosed ligand was used for the assay based on DNA-tagged bromodomain). Importantly, the ligand efficiency of compounds **1** and **3** is very favorable irrespective of the assay (Table 1).

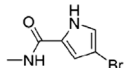
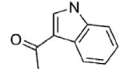
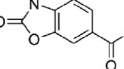
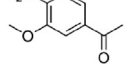
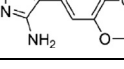
In our previous fragment-based high-throughput docking campaigns for the bromodomains of BRD4 (N-terminal),²⁶ CBP,¹³ BRPF1,²¹ BAZ2A (PDB codes 5MGJ, 5MGK, 5MGL, 5MGM), BAZ2B,^{27,28} and ATAD2 (PDB codes 5EPB, 5F3A, 5F36) the poses predicted by docking were validated by protein crystallography. Similarly, in the present VS2NMR campaign, we decided to validate the binding poses predicted by docking by means of X-ray crystallography. Towards this goal, we solved the crystal structures of the complexes of the CBP bromodomain with ligands **1** to **4** at resolution of 1.65 Å or higher (Figs. 2 and S4, Table S2).

Compound **1** forms four hydrogen bonds with the CBP bromodomain (Fig. 2A). There are two direct hydrogen bonds involving the pyrrole NH and carbonyl oxygen acting as donor and acceptor, respectively, for the side chain of the conserved Asn1168. Furthermore, two water-mediated hydrogen bonds are formed between the carbonyl oxygen of compound **1** and the side chain hydroxyl of the conserved Tyr1125 (through the structural water w_1) and between the NH of the carboxamide and the backbone carbonyl of Pro1110. The bromine substituent of **1** points towards the side chains of Leu1120 and Ile1122 in the ZA-loop, which provides stabilization by hydrophobic contacts. The pose predicted by docking is consistent with the binding mode in the crystal structure except for the relative orientation of the pyrrole and the N-methylamide, which is due to the conformer used for docking and the rigid-ligand docking protocol.

As for compound **1**, a minor discrepancy between docked pose and binding mode in the crystal structure is observed for compound **3** (Fig. 2C) which is again a consequence of the different conformer used in the rigid-docking protocol. Importantly, the position of the double-ring system and the two hydrogen bonds of the carbonyl oxygen (with the side chain of Asn1168 and the water w_1) are predicted correctly by docking. Interestingly, a second molecule **3** is present outside of the Kac binding site, with stabilization due to stacking between the indole of Trp1151 and the phenyl of Tyr1102 of a neighboring CBP bromodomain, and a hydrogen bond with the side chain of Gln1113 of the same neighboring protein (Fig. 3). Thus, the second binding mode is stabilized by crystal packing.

The pose predicted by docking for the 3-acetylindole **2** and acetylbenzene derivative **4** are essentially identical to the binding mode in the crystal structures (Fig. 2B,D). The methoxy oxygen of the acetylbenzene derivative **4** is involved in a water-bridged hydrogen bond with the backbone oxygen of Pro1110 (Fig. 2D) or the side chain oxygen of Asn1168 (Fig. S5) in the two protein chains of the asymmetric unit. As expected, the binding pose of **4** superimposes with an acetylbenzene-based sub-micromolar inhibitor reported recently (PDB code 4TQN, Fig. S6).¹³ In both struc-

Table 1
In silico identified ligands of the CBP bromodomain.

| | 2D structure | HAC ^a | PDB code | DSF (°C) ^b | | AlphaScreen | | | BROMOscan | |
|---|---|------------------|----------|-----------------------|-------|----------------|------------------------|-----------------|----------------------------------|-----------------|
| | | | | CBP | EP300 | % ^c | IC50 (μM) ^d | LE ^e | K _D (μM) ^f | LE ^e |
| 1 |  | 10 | 5MQE | 7.3 | 7.0 | 0.1 | 40 | 0.60 | 4 | 0.74 |
| 2 |  | 13 | 5MQK | 2.9 | 2.6 | 31 | n.d. ^g | n.d. | n.d. | n.d. |
| 3 |  | 14 | 5MPZ | 2.3 | 1.4 | 34 | 455 | 0.33 | 85 | 0.40 |
| 4 |  | 12 | 5MQG | 2.4 | 2.6 | 37 | n.d. | n.d. | n.d. | n.d. |
| 5 |  | 16 | – | –0.1 | –1.3 | 48 | n.d. | n.d. | n.d. | n.d. |

^a HAC: heavy atom count.

^b Differential scanning fluorimetry (DSF) measurements were carried out at a bromodomain concentration of 2 μM and a ligand concentration of 1 mM. For each ligand/bromodomain pair, the shift in the melting temperature is the median value of at least nine measurements. Standard error of the mean values were smaller than 0.3 °C in all cases.

^c Binding of the CBP bromodomain to a labelled acetylated peptide in the presence of 0.5 mM of the ligand with respect to DMSO solution, with lower percentage values indicating stronger inhibition.

^d IC50 values were determined by curve fitting of 10-point dose responses.

^e Ligand efficiency (LE) values are reported in kcal/mol per heavy atom.

^f K_D values, as determined by curve fitting of 12-point dose responses in duplicates in a competition-binding experiment based on DNA-tagged CBP bromodomain and quantitative PCR.¹⁵

^g n.d.: not determined.

tures, the acetyl oxygen of the ligand acts as acceptor in a direct hydrogen bond with the side chain NH₂ of the conserved Asn1168 and a water-bridged hydrogen bond to the side chain of Tyr1125. As reported previously,^{21,29,30} the distance between the acetyl oxygen and the bridging water (2.7 Å for both compounds **2** and **4**) is shorter than the distance to the nitrogen atom of the Asn1168 side chain (3.0 Å). A shorter distance to the bridging w₁ oxygen than the Asn1168 side chain nitrogen is also observed for the carbonyl oxygen of compounds **1** and **3** (Fig. S7).

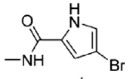
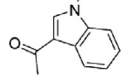
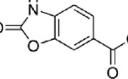
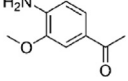
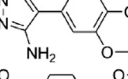
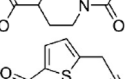
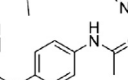
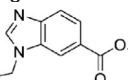
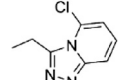
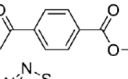
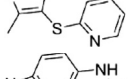
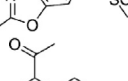
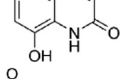
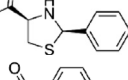
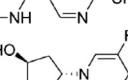
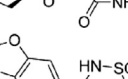
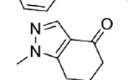
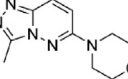
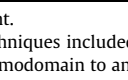
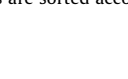
An essential element of our fragment-docking procedure is the efficient evaluation of the binding energy which is the sum of the van der Waals interaction and electrostatic energy in the continuum dielectric approximation (see original papers on the SEED software).^{16,17} The electrostatic contribution to the binding energy is the sum of the screened interaction between the (partial) charges in the protein and the ligand, and the desolvation penalty of the receptor and fragment upon binding. It is useful to analyze the individual contributions to the binding energy. Here, we focus the analysis on the top two poses (according to total binding energy as calculated by SEED) as the third ranking pose was significantly less favorable for the four fragment hits **1–4**. The total SEED energy favors the pose that is close to the binding mode observed in the crystal structure (Fig. 4). On the other hand, the van der Waals contribution does not consistently favor the binding mode observed in the crystal structure. The van der Waals energy is always favorable because it consists of only the fragment/protein contribution, while the loss of solute/solvent van der Waals energy upon binding is neglected. In contrast, the electrostatic contribution to the binding energy (ΔG_{elec}), which includes desolvation effects, always favors the pose close to the binding mode observed in the crystal structure over the second best pose. More precisely, for compound **3** the desolvation penalty is less unfavorable for the top pose than the second best pose while for compounds **1**, **2**, and **4** it is rather the intermolecular electrostatic contribution that favors the top pose. This analysis provides evidence that a simple scoring

function, e.g., based on only van der Waals energy, would not have sufficient predictive ability. It also highlights the importance of the evaluation of the electrostatic energy with solvation for identifying the correct binding mode among the multiple poses generated by docking.

In conclusion, we efficiently identified inhibitors of the CBP bromodomain by means of a VS2NMR campaign using high-throughput fragment docking (by the program SEED)^{16,17} followed by ligand-observed NMR spectroscopy. First, the initial 1413 fragments were reduced to 39 candidate ligands by *in silico* screening, which required only two hours of a commodity computer. Twenty of these molecules showed specific, competitive binding in ligand-observed NMR experiments. In contrast to the present study in which NMR measurements were performed on a small set of molecules preselected by high-throughput docking, in previous reports by others NMR spectroscopy has been employed as primary screening with the following protocols: 2D HSQC or HMQC NMR,^{31–36} ligand-observed NMR,^{37,38} protein observed fluorine NMR,^{39,40} and target immobilized NMR screening.⁴¹ Importantly, with the present VS2NMR campaign, 50% of the small molecules predicted by docking as candidate ligands of the CBP bromodomain were confirmed by ligand-observed NMR spectroscopy, a higher success ratio than that of primary NMR screens on bromodomains, which range from 0.3%³³ to 13.5%.⁴⁰ Although it is not possible to directly compare different screening protocols and targets, the present study provides evidence that the VS2NMR strategy is time and resource efficient. As a matter of fact, the primary screening of nearly 1500 compounds by NMR, including data analysis, would have required about three weeks, while the present VS2NMR campaign took about two days.

We have recently carried out a VS2NMR campaign for the BAZ2A bromodomain starting from the same 1413-fragment library as in the present study and with the same validation by ligand-based NMR as secondary screening (D. Spiliotopoulos et al., manuscript in preparation). The success ratio for CBP (20

Table 2
Ligand-based NMR spectroscopy validation of the molecules predicted *in silico* as CBP bromodomain ligands.

| | 2D structure | HAC ^a | NMR screening ^b | | | AlphaScreen % ^c |
|----|---|------------------|----------------------------|-----|------|----------------------------|
| | | | ¹ H | STD | CPMG | |
| 1 |  | 10 | + | + | + | 0.1 |
| 2 |  | 13 | - | + | + | 31 |
| 3 |  | 14 | + | + | + | 34 |
| 4 |  | 11 | + | + | + | 37 |
| 5 |  | 16 | - | - | + | 48 |
| 6 |  | 12 | - | - | + | 56 |
| 7 |  | 11 | + | - | + | 56 |
| 8 |  | 14 | + | + | + | 74 |
| 9 |  | 15 | + | + | + | 79 |
| 10 |  | 12 | + | + | + | 85 |
| 11 |  | 12 | - | + | + | 92 |
| 12 |  | 13 | + | - | + | 92 |
| 13 |  | 15 | - | + | + | 92 |
| 14 |  | 15 | + | + | + | 93 |
| 15 |  | 15 | + | - | + | 94 |
| 16 |  | 14 | - | - | + | 96 |
| 17 |  | 17 | + | - | + | 98 |
| 18 |  | 15 | - | - | + | 100 |
| 19 |  | 11 | + | + | + | 100 |
| 20 |  | 17 | - | - | + | 102 |

^a HAC: heavy atom count.

^b NMR spectroscopy techniques included ¹H, saturation transfer difference (STD) NMR and Carr-Purcell-Meiboom-Gill (CPMG).

^c Binding of the CBP bromodomain to an acetylated peptide in the presence of 0.5 mM of the ligand with respect to DMSO solution, with lower values indicating stronger inhibition. The compounds are sorted according to percentage binding.

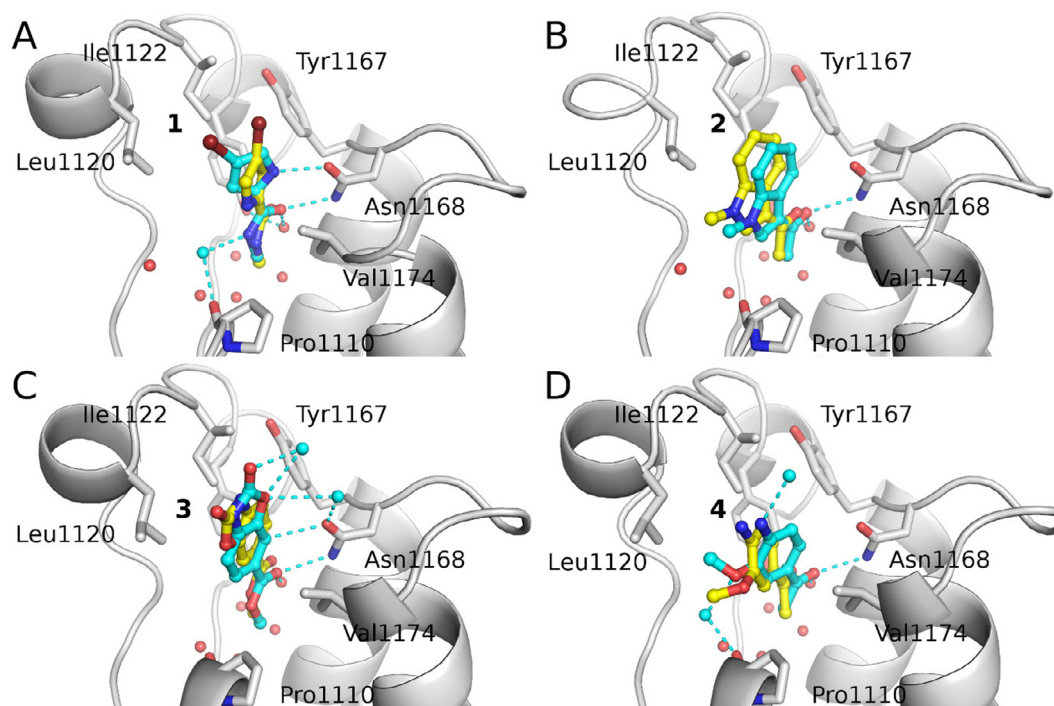


Fig. 2. Structural validation of the fragment-based *in silico* screening campaign for CBP. (A–D) The binding mode in the crystal structures (carbon atoms of ligands in cyan) are compared to the binding pose predicted by docking with SEED^{16,17} (carbon atoms in yellow) for compounds (A) **1**, (B) **2**, (C) **3**, and (D) **4** (PDB codes: 5MQE, 5MQK, 5MPZ, and 5MQG, respectively). Conserved water molecules and water molecules present in the crystal structure but not used for docking are shown as red and cyan spheres, respectively. Compounds **1** and **3** have a different relative orientation of the substituents, which could not be predicted by SEED since the compounds were docked as rigid molecules.

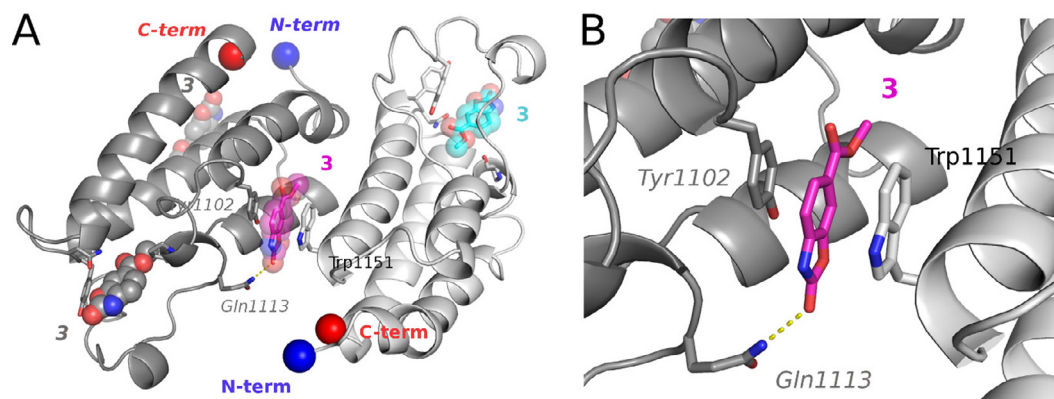


Fig. 3. Two molecules of compound **3** bind to the CBP bromodomain in the crystal structure. (A) The two compound **3** molecules present in the crystallographic unit of the CBP/**3** complex (gray cartoons) are shown as sticks and transparent spheres. A description of the pose of the molecule bound to the Kac-binding site (carbon atoms in cyan or gray) can be found in the text. The second molecule (magenta) stacks between the side chains of Trp1151 and Tyr1102 of a neighboring CBP bromodomain. The N- and C-termini of the bromodomains are shown with a blue and red sphere, respectively. (B) Zoom on the additional compound **3** molecule and the protein residues surrounding it. The polar interaction between the carbonyl oxygen of the ligand and the side chain of the Gln1113 of the neighboring CBP bromodomain is shown with dashed lines. The two bromodomains are shown with dark and light gray, respectively.

actives according to NMR out of 39 candidate ligands) is higher than for the BAZ2A bromodomain (7 actives out of 20 candidate ligands) which is a more difficult target as it has a shallower Kac binding site.

The high ligand efficiency of the *in silico* identified fragments calls for hit expansion. In a cellular *milieu*, the methylester of compound **3** is likely to be converted into a carboxyl group. The resulting negative charge on the carboxyl group would hinder binding to the Kac pocket because of the electrostatic desolvation penalty. On the other hand, the binding mode of the brominated pyrrole **1** is compatible with fragment growing by Suzuki coupling.

Author contribution

J. A. and C. R. compiled the library of compounds and J.-R. M. parametrized it. D.S. and A.C. performed and analyzed the virtual screening. N. D. purified the protein samples for the NMR screening and performed and analyzed the DSF measurements. E.-C. W. and D. S. performed and analyzed the NMR screen. J. Z. purified the protein for X-ray crystallography, grew the crystals and solved the structures. D.S. and A.C. wrote the manuscript with contributions from all authors.

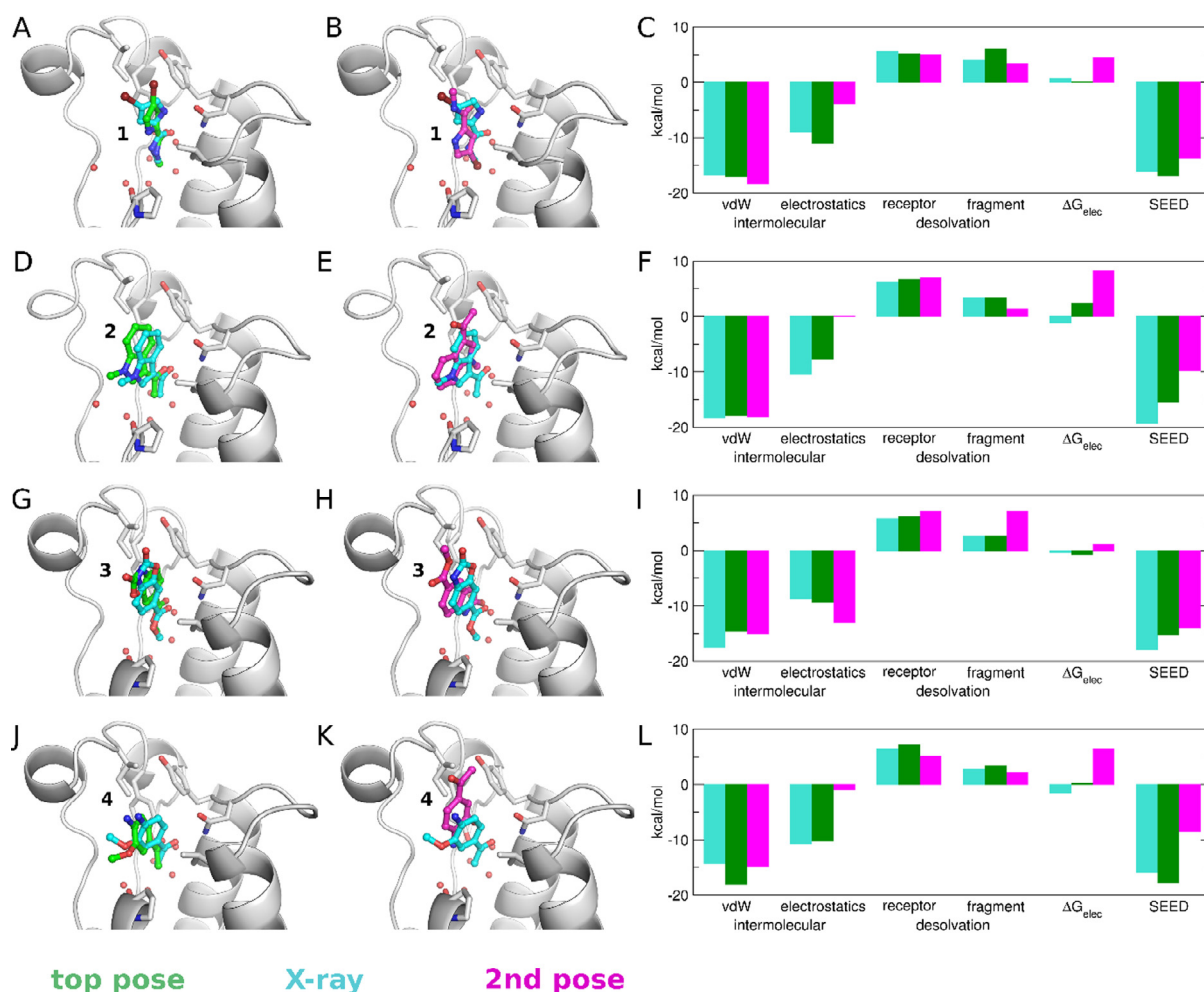


Fig. 4. Insights into the energetic terms calculated using SEED for the two top poses of compounds **1** (A–C), **2** (D–F), **3** (G–I), and **4** (J–L). The CBP bromodomain is shown as a cartoon and sticks with white carbon atoms, whereas the ligands are shown as sticks. The color coding is consistent in all panels (cyan, green, and magenta for binding mode in the crystal structure, top pose and 2nd best pose according to total SEED energy, respectively). (C, F, I, L) The contributions to the binding energy are the intermolecular van der Waals energy, the intermolecular electrostatics energy calculated in the solvent using a continuum dielectric representation, the electrostatic desolvation energy of the receptor and ligand upon binding. These terms sum up to the total energy. The electrostatic contribution to the binding free energy in the solvent (ΔG_{elec}) is the sum of intermolecular electrostatic energy and desolvation penalties.

Accession codes

Structure were deposited to the PDB with accession numbers 5MQE (CBP/1), 5MQK (CBP/2), 5MPZ (CBP/3), and 5MQG (CBP/4).

Conflict of interest

The authors declare no competing interest.

Acknowledgements

We thank the Structural Genomics Consortium at University of Oxford for providing the plasmid of the CBP bromodomain. EP300 was a gift from Nicola Burgess-Brown (Addgene plasmid # 39018). The AlphaScreen and BROMOScan measurements were performed at Reaction Biology Corporation and DiscoverX, respectively. This work was supported in part by the Swiss National Science Foundation (grant to A.C.) and Max Planck Society and the German Research Foundation (DFG, RA1944/2-1) (C.R., J. A. and E.W.). D.S. is a recipient of the SystemsX.ch translational postdoc fellowship and gratefully acknowledges support from the Holcim Foundation.

A. Supplementary data

Supplementary data associated with this article can be found, in the online version, at <http://dx.doi.org/10.1016/j.bmcl.2017.04.001>.

References

- Dhalluin C, Carlson JE, Zeng L, He C, Aggarwal AK, Zhou MM. Structure and ligand of a histone acetyltransferase bromodomain. *Nature*. 1999;399(6735):491–496.
- Flynn EM, Huang OW, Poy F, et al. A subset of human bromodomains recognizes butyryllysine and crotonyllysine histone peptide modifications. *Structure*. 2015;23(10):1801–1814.
- Zhang G, Smith SG, Zhou MM. Discovery of chemical inhibitors of human bromodomains. *Chem Rev*. 2015;115(21):11625–11668.
- Filippakopoulos P, Knapp S. Targeting bromodomains: Epigenetic readers of lysine acetylation. *Nat Rev Drug Discov*. 2014;13(5):337–356.
- Müller S, Filippakopoulos P, Knapp S. Bromodomains as therapeutic targets. *Expert Rev Mol Med*. 2011;13:e29.
- Ferri E, Petosa C, McKenna CE. Bromodomains: structure, function and pharmacology of inhibition. *Biochem Pharmacol*. 2016;106:1–18.
- Iyer NG, Ozdag H, Caldas C. P300/CBP and cancer. *Oncogene*. 2004;23(24):4225–4231.
- Hay DA, Fedorov O, Martin S, et al. Discovery and optimization of small-molecule ligands for the CBP/p300 bromodomains. *J Am Chem Soc*. 2014;136(26):9308–9319.

9. Rooney TP, Filippakopoulos P, Fedorov O, et al. A series of potent CREBBP bromodomain ligands reveals an induced-fit pocket stabilized by a cation- π interaction. *Angew Chem Int Ed*. 2014;53(24):6126–6130.
10. Picaud S, Fedorov O, Thanasopoulou A, et al. Generation of a selective small molecule inhibitor of the CBP/p300 bromodomain for leukemia therapy. *Cancer Res*. 2015;75(23):5106–5119.
11. Taylor AM, Cote A, Hewitt MC, et al. Fragment-based discovery of a selective and cell-active benzodiazepinone CBP/EP300 bromodomain inhibitor (CPI-637). *ACS Med Chem Lett*. 2016;7(5):531–536.
12. Crawford TD, Romero FA, Lai KW, et al. Discovery of a potent and selective in vivo probe (GNE-272) for the bromodomains of CBP/EP300. *J Med Chem*. 2016;59(23):10549–10563.
13. Xu M, Unzue A, Dong J, Spiliotopoulos D, Nevado C, Caffisch A. Discovery of CREBBP bromodomain inhibitors by high-throughput docking and hit optimization guided by molecular dynamics. *J Med Chem*. 2016;59(4):1340–1349.
14. Unzue A, Xu M, Dong J, et al. Fragment-based design of selective nanomolar ligands of the CREBBP bromodomain. *J Med Chem*. 2016;59(4):1350–1356.
15. Quinn E, Wodicka L, Ciceri P, et al. BROMOScan – a high throughput, quantitative ligand binding platform identifies best-in-class bromodomain inhibitors from a screen of mature compounds targeting other protein classes. *Cancer Res*. 2013;73:4238.
16. Majeux N, Scarsi M, Apostolakis J, Ehrhardt C, Caffisch A. Exhaustive docking of molecular fragments with electrostatic solvation. *Proteins*. 1999;37:88–105.
17. Majeux N, Scarsi M, Caffisch A. Efficient electrostatic solvation model for protein-fragment docking. *Proteins*. 2001;42(2):256–268.
18. Aretz J, Wamhoff EC, Hanske J, Heymann D, Rademacher C. Computational and experimental prediction of human C-type lectin receptor druggability. *Front Immunol*. 2014;5:323.
19. Mayer M, Meyer B. Characterization of ligand binding by saturation transfer difference NMR spectroscopy. *Angew Chem Int Ed*. 1999;38(12):1784–1788.
20. Hajduk PJ, Olejniczak ET, Fesik SW. One-dimensional relaxation- and diffusion-edited NMR methods for screening compounds that bind to macromolecules. *J Am Chem Soc*. 1997;119(50):12257–12261.
21. Zhu J, Caffisch A. Twenty crystal structures of bromodomain and PHD finger containing protein 1 (BRPF1)/ligand complexes reveal conserved binding motifs and rare interactions. *J Med Chem*. 2016;59(11):5555–5561.
22. Philpott M, Yang J, Tumber T, et al. Bromodomain-peptide displacement assays for interactome mapping and inhibitor discovery. *Mol BioSyst*. 2011;7(10):2899–2908.
23. Theodoulou NH, Bamborough P, Bannister AJ, et al. Discovery of I-BRD9, a selective cell active chemical probe for bromodomain containing protein 9 inhibition. *J Med Chem*. 2016;59(4):1425–1439.
24. Crawford TD, Tsui V, Flynn EM, et al. Diving into the water: inducible binding conformations for BRD4, TAF1(2), BRD9, and CECR2 bromodomains. *J Med Chem*. 2016;59(11):5391–5402.
25. Tanaka M, Roberts JM, Seo HS, et al. Design and characterization of bivalent BET inhibitors. *Nat Chem Biol*. 2016;12(12):1089–1096.
26. Zhao H, Gartenmann L, Dong J, Spiliotopoulos D, Caffisch A. Discovery of BRD4 bromodomain inhibitors by fragment-based high-throughput docking. *Bioorg Med Chem Lett*. 2014;24(11):2493–2496.
27. Lolli G, Caffisch A. High-throughput fragment docking into the BAZ2B bromodomain: efficient in silico screening for X-ray crystallography. *ACS Chem Biol*. 2016;11(3):800–807.
28. Marchand JR, Lolli G, Caffisch A. Derivatives of 3-amino-2-methylpyridine as BAZ2B bromodomain ligands: in silico discovery and in crystallo validation. *J Med Chem*. 2016;59(21):9919–9927.
29. Chung C-W, Dean AW, Woolven JM, Bamborough P. Fragment-based discovery of bromodomain inhibitors part 1: inhibitor binding modes and implications for lead discovery. *J Med Chem*. 2011;55(2):576–586.
30. Marchand JR, Caffisch A. Binding mode of acetylated histones to bromodomains: variations on a common motif. *ChemMedChem*. 2015;10(8):1327–1333.
31. Zeng L, Li J, Muller M, et al. Selective small molecules blocking HIV-1 Tat and coactivator PCAF association. *J Am Chem Soc*. 2005;127(8):2376–2377.
32. Sachchidanand, Resnick-Silverman L, Yan S, et al. Target structure-based discovery of small molecules that block human p53 and CREB binding protein association. *Chem Biol*. 2006;13(1):81–90.
33. Borah JC, Mujtaba S, Karakikes I, et al. A small molecule binding to the coactivator CREB-binding protein blocks apoptosis in cardiomyocytes. *Chem Biol*. 2011;18(4):531–541.
34. Harner MJ, Frank AO, Fesik SW. Fragment-based drug discovery using NMR spectroscopy. *J Biomol NMR*. 2013;56(2):65–75.
35. Chaikwad A, Petros AM, Fedorov O, Xu J, Knapp S. Structure-based approaches towards identification of fragments for the low-druggability ATAD2 bromodomain. *Med Chem Commun*. 2014;5(12):1843–1848.
36. Ghosh S, Taylor A, Chin M, et al. Regulatory T cell modulation by CBP/EP300 bromodomain inhibition. *J Biol Chem*. 2016;13014–13027.
37. Demont EH, Bamborough P, Chung CW, et al. 1,3-Dimethyl benzimidazolones are potent, selective inhibitors of the BRPF1 bromodomain. *ACS Med Chem Lett*. 2014;5(11):1190–1195.
38. Wang N, Li F, Bao H, Li J, Wu J, Ruan K. NMR Fragment screening hit induces plasticity of BRD7/9 bromodomains. *ChemBioChem*. 2016;17(15):1456–1463.
39. Mishra NK, Urlick AK, Ember SW, Schonbrunn E, Pomerantz WC. Fluorinated aromatic amino acids are sensitive 19F NMR probes for bromodomain-ligand interactions. *ACS Chem Biol*. 2014;9(12):2755–2760.
40. Urlick AK, Hawk LM, Cassel MK, et al. Dual screening of BPTF and Brd4 using protein-observed fluorine NMR uncovers new bromodomain probe molecules. *ACS Chem Biol*. 2015;10(10):2246–2256.
41. Chaikwad A, Lang S, Brennan PE, et al. Structure-based identification of inhibitory fragments targeting the p300/CBP-associated factor bromodomain. *J Med Chem*. 2016;59(4):1648–1653.